Quasi-BIC Resonant Enhancement of Second-Harmonic Generation in WS_2 Monolayers

Nils Bernhardt,[†,‡,#] Kirill Koshelev,[¶,§,#] Simon White,[†] Kelvin Wong Choon Meng,[†,‖] Johannes E. Fröch,[†] Sejeong Kim,[†] Toan Trong Tran,[†] Duk-Yong Choi,[⊥] Yuri Kivshar,[*,¶,§] and Alexander S. Solntsev[*,†]

†*School of Mathematical and Physical Sciences, University of Technology Sydney, Sydney NSW 2007, Australia*

‡*Institut für Optik und Atomare Physik, Technische Universität Berlin, Berlin 10623, Germany*

¶*Nonlinear Physics Center, Research School of Physics, Australian National University, Canberra ACT 2601, Australia*

§*Department of Physics and Engineering, ITMO University, St Petersburg 197101, Russia*

‖*Republic Polytechnic, 738964, Singapore*

⊥*Laser Physics Center, Research School of Physics, Australian National University, Canberra ACT 2601, Australia*

#*Contributed equally to this work*

E-mail: yuri.kivshar@anu.edu.au; alexander.solntsev@uts.edu.au

Abstract

Atomically thin monolayers of transition metal dichalcogenides (TMDs) emerged as a promising class of novel materials for optoelectronics and nonlinear optics. However, the intrinsic nonlinearity of TMD monolayers is weak, limiting their functionalities for nonlinear optical processes such as frequency conversion. Here, we boost the effective nonlinear susceptibility of a TMD monolayer by integrating it with a resonant dielectric metasurface, which supports pronounced optical resonances with high quality factors: bound states in the continuum (BICs). We demonstrate that a WS_2 monolayer combined with a silicon metasurface hosting BICs can enhance the second-harmonic intensity by more than three orders of magnitude compared to a WS_2 monolayer on top of a flat silicon film of the same thickness. Our work suggests a pathway to employ high-index dielectric metasurfaces as hybrid structures for enhancement of TMD nonlinearities with applications in nonlinear microscopy, optoelectronics, and signal processing.

Keywords

all-dielectric metasurfaces, two-dimensional material, nanophotonics, bound states in the continuum, second-harmonic generation

Introduction

Atomically thin two-dimensional (2D) materials beyond graphene, such as monolayers of transition metal dichalcogenides (TMDs), have attracted widespread attention in recent years because their electronic and optical properties enable new functionalities beyond capabilities of conventional bulk materials.[1] Optically, 2D TMD monolayers are characterized by a direct bandgap enabling strong luminescence.[2] Moreover, these structures support excitons characterized by both considerable binding energies and sufficiently large Bohr radii,

enabling strong excitonic response at room temperature.[3] The optically-accessible valley degree of freedom in these structures further renders them a very compelling class of materials for information processing and storage.[4] Recently, observation of nonlinear optical processes with TMD monolayers, such as second-harmonic generation (SHG), has attracted a special research interest,[5–8] as these materials are inherently non-centrosymmetric. Second-harmonic (SH) microscopy has also become a recognized method to determine the crystalline structure, the presence of defects, and a number of atomic layers.[9–12] Although an SH signal from a TMD monolayer is observable, the overall frequency conversion efficiency is limited by the atomic length of the interaction with light, thus preventing their future practical applications.

The integration of 2D materials with various resonant and waveguiding photonic structures has been shown to provide a promising way for achieving higher efficiencies of nonlinear optical processes.[13–16] Plasmonic materials are traditionally associated with high material losses and low damage thresholds, which both limit their functionality for nonlinear applications. Recently, all-dielectric resonant meta-structures with high refractive index have emerged as an alternative platform to complement and even outperform the capabilities of plasmonic materials benefiting from low optical losses governed by radiation leakage only.[17–19] In particular, a recently developed concept of bound states in the continuum (BICs) in nanophotonics[20,21] enables a simple approach to engineer radiative losses for various all-dielectric structures, ranging from isolated nanoparticles to extended periodic ensembles, to achieve sharp resonances with a high quality factor (Q factor) in the form of quasi-BICs.[22–25] Moreover, very recently, it was revealed that thin metasurfaces created of dielectric meta-atoms with broken in-plane inversion symmetry could support high-quality quasi-BICs with radiative Q factors depending on the asymmetry of the unit cell.[26]

Here, for the first time to our knowledge, we demonstrate a sharp enhancement of SHG from a 2D material coupled to a spatially extended quasi-BIC resonance excited optically in a dielectric metasurface. For this, we use a tungsten-disulfide (WS_2) monolayer placed on

top of a Si metasurface with broken in-plane inversion symmetry (Figure 1a). We engineer the asymmetry of the meta-atoms to achieve the regime of critical coupling[27] with balanced rates of radiative losses and all other losses, which provides the maximal field enhancement inside the WS_2 monolayer. We fabricate a set of metasurfaces with different asymmetry parameters and analyze them with SH spectroscopy to select the sample tuned to the critical coupling regime. We then transfer WS_2 flakes on top of the optimized metasurface and a reference bare Si film of the same thickness. We confirm a high quality of WS_2 monolayers by photoluminescence (PL) measurements. Finally, we experimentally demonstrate the enhancement of SHG from the monolayer placed on a metasurface substrate of at least 1140 times compared to a bulk Si substrate – more than one and a half orders of magnitude higher than that demonstrated earlier for resonant metasurfaces[28] and nearly an order of magnitude above the best cases utilizing other approaches.[13,16] By demonstrating the giant enhancement in the SHG emission from a WS_2 monolayer, we have tackled one of the critical limitations of TMD monolayers for practical implementations in nonlinear optics – their low frequency-conversion efficiency due to one-atom effective interaction length.[15] Our demonstration opens up a new avenue for the deployment of TMD monolayers for efficient integrated nonlinear photonic and optoelectronics devices.[29,30]

Results and Discussion

Our hybrid photonic structure is based on a Si metasurface composed of a square lattice of bar pairs and a WS_2 monolayer placed on top of the metasurface. The material choice for the metasurface is explained by mature fabrication technology and centrosymmetric atomic structure of silicon, which prohibits intrinsic SHG from the material. Each meta-atom consists of two parallel bars of slightly different widths, and the asymmetry parameter α is defined as a ratio between the width difference dL and width of a larger bar L (see Figure 1b). Below the diffraction limit, the metasurface supports several distinct quasi-BIC

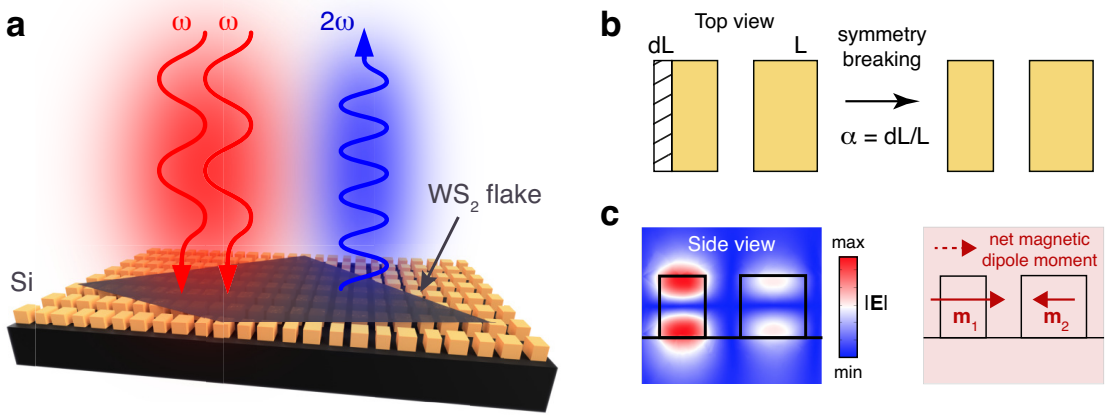

Figure 1: Hybrid photonic structure for the enhanced harmonic generation. (a) Schematic of SHG from a WS_2 monolayer placed on top of a Si metasurface composed of a square array of bar pairs. (b) Design of the unit cell with the definition of the asymmetry parameter α. (c) Near-field distribution of the electric field of quasi-BIC inside the meta-atom (left), and magnetic dipole moments of the individual resonators $\mathbf{m}_1$ and $\mathbf{m}_2$ with the net magnetic dipole moment of the unit cell (right).

resonances with high Q factors and different field profiles and polarizations, which originate from distortion of symmetry-protected BICs via asymmetry ($\alpha \neq 0$).[26] We focus on the quasi-BIC with a field pattern of an in-plane polarized magnetic dipole (Figure 1c). The origin of the magnetic dipole pattern is the net magnetic dipole moment of two adjacent bars. Such an electric field distribution is localized near the bar surface, providing high field enhancement inside the 2D material.

The field enhancement at the resonance depends on the interplay between different mechanisms of mode losses.[31] We engineer the loss rates of the quasi-BIC via control of the meta-atom asymmetry, which allows maximizing the electric field inside the TMD layer. Figure 2a schematically shows various mechanisms of losses of the quasi-BIC mode in realistic conditions taking fabrication errors into account. Below the diffraction limit, the quasi-BIC radiates with the rate γ_{rad} into a single diffraction channel, which describes the radiation normal to the surface plane. The rate γ_{rad} increases with the asymmetry parameter quadratically, $\gamma_{\text{rad}} \propto \alpha^2$.[26] We denote other mechanisms of losses, including material absorption, scattering due to surface roughness, and radiation from the edges, as parasitic with the

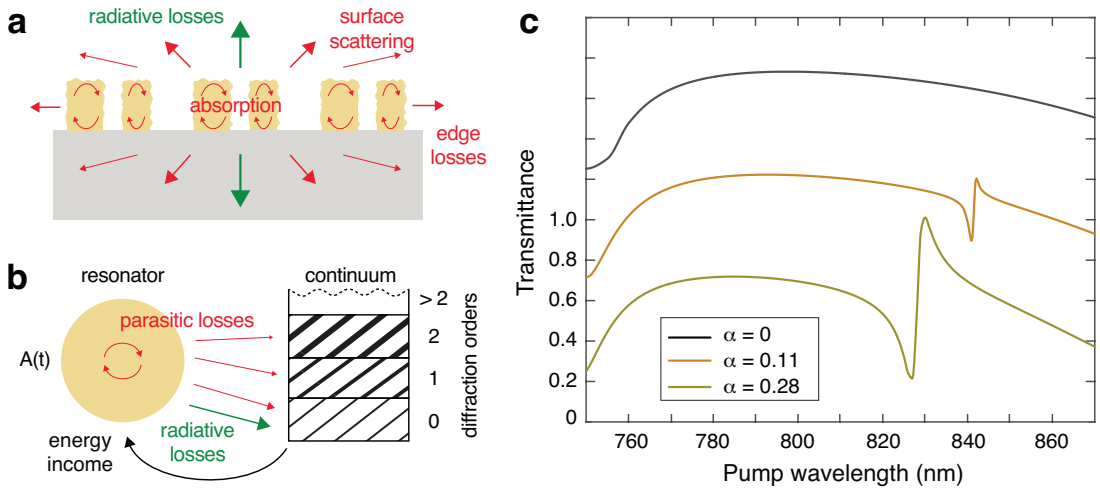

Figure 2: (a) Schematic representation of radiative (green) and parasitic (red) losses of the quasi-BIC mode for a realistic sample of finite size with fabrication imperfections. (b) Schematic of the evolution of resonant amplitude of the quasi-BIC $A(t)$ [see Eq. (1)] coupled to the radiation continuum via radiation to the zeroth diffraction order (green) and parasitic losses (red) due to absorption and scattering to all diffraction orders. (c) Simulated evolution of the metasurface transmittance with respect to the meta-atom asymmetry. The spectra are relatively shifted by 0.5 units.

rate γ_{par} because they originate from material and fabrication imperfections.[32] For dielectric metasurfaces, surface roughness, spatial disorder, and sample edges can add extra in-plane momentum to the quasi-BIC,[24] which induces parasitic scattering γ_{par} to nonzero angles and even high-order diffraction channels. We note that γ_{par} is robust to small changes of α. The total rate of quasi-BIC losses γ is given by a sum of all contributions $\gamma = \gamma_{\text{rad}} + \gamma_{\text{par}}$.

For qualitative analysis of the effect of losses on the field enhancement, we use the temporal coupled-mode theory.[33] We are interested in the wavelength range around 830 nm, for which the WS_2 monolayer is non-resonant because its excitonic resonances are at the wavelengths below 630 nm.[34] We consider a single-mode resonator tuned to a quasi-BIC mode, whose resonant amplitude $A(t)$ changes in time due to self-oscillations and excitation by an external pump (Figure 2b),

$$\frac{dA(t)}{dt} = -i[\omega - i(\gamma_{\text{rad}} + \gamma_{\text{par}})]A(t) + \kappa E_0. \tag{1}$$

Here, ω is the real part of the quasi-BIC frequency, E_0 is the amplitude of the pump electric field, and κ is the amplitude of coupling between the pump and the quasi-BIC.

The sub-diffractive regime and reciprocity allow to relate κ to the rate of radiative losses[33] as $\kappa \propto \gamma_{\mathrm{rad}}^{1/2}$. The parasitic losses are contributed by material absorption and scattering to different states of the continuum, including high-order diffraction (Figure 2b). The field enhancement $|u|^2$ at the resonance is given by the relative magnitude of the loss rates (see Supporting Information),

$$|u|^2 = \frac{|A|^2}{E_0^2} \propto \frac{\gamma_{\mathrm{rad}}(\alpha)}{\left[\gamma_{\mathrm{rad}}(\alpha) + \gamma_{\mathrm{par}}\right]^2}. \tag{2}$$

Here, γ_{rad} has pronounced dependence on the asymmetry parameter.

Analysis of Eq. (2) shows that for constant γ_{par} the maximal field enhancement is achieved for the condition $\gamma_{\mathrm{rad}} = \gamma_{\mathrm{par}}$, which is often termed as the critical coupling condition.[27] The rate of radiative losses depends directly on α, and it can be tuned to match the rate of parasitic losses determined solely by the manufacturing process and material properties. Equation (2) shows that for the critical coupling condition, the field enhancement A^2/E_0^2 scales linearly with the mode Q factor $Q = \omega/\gamma$. We also note that we omitted the dependence on the mode volume because it changes slowly with α.

Next, we design the metasurface parameters for further fabrication and experimental analysis. We engineer a quasi-BIC at a wavelength of 832 nm, for which the intrinsic nonlinear susceptibility of a WS_2 monolayer has a local maximum, and silicon is transparent. For simulations, we consider an infinite square array of bar pairs; the period is 500 nm, height is 160 nm, each bar length is 245 nm, larger bar width is 180 nm, and the distance between the bars is 100 nm. To find a proper design, we vary the width of the smaller bar in the range of 130, 160, and 180 nm, which corresponds to $\alpha \simeq 0.28$, 0.11, and 0, respectively. The simulated transmittance for each metasurface is shown in Figure 2c. For $\alpha = 0.28$, a quasi-BIC appears at 830 nm, and it manifests itself as a sharp asymmetric resonance. For a fully symmetric unit cell ($\alpha = 0$), this resonant feature disappears.

We use the target design to fabricate a set of metasurfaces with different asymmetry

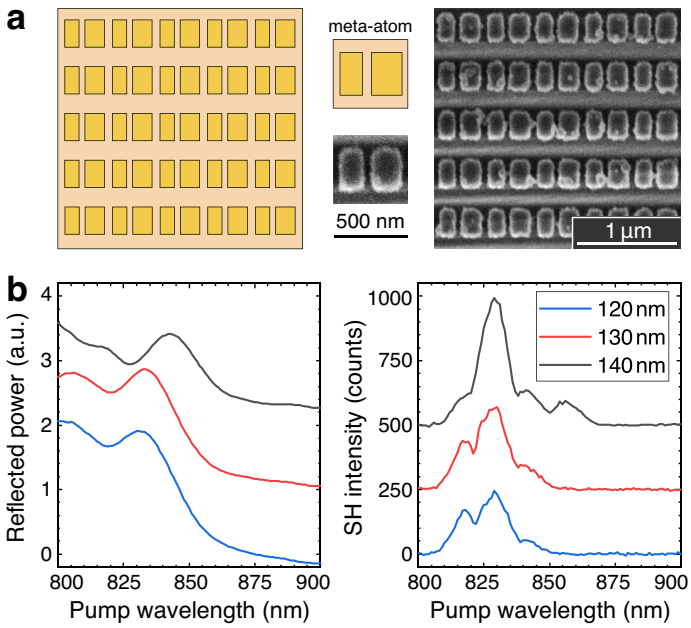

Figure 3: (a) Schematic view and SEM image of the fabricated Si metasurface, top view. The inset shows the designed and fabricated meta-atoms. (b) Measured linear reflected power and second-harmonic intensity vs. pump wavelength for three different metasurface samples, with a width of the smaller bar of 120, 130, 140 nm, respectively. The linear and SH spectra are shifted by 1.2 units, and 250 counts, respectively.

parameters to achieve the critical coupling regime. The meta-atoms are fabricated from hydrogenated amorphous Si on a transparent substrate with the pattern size of 30 µm × 30 µm and smaller bar width varying from 120 to 140 nm (Figure 3a). Additionally, a 50 µm × 50 µm bulk Si film of the same thickness as a reference sample was fabricated for further comparison of the SHG efficiencies. We measure the reflection spectrum from metasurfaces with a laser tunable within the wavelength range of 800 to 900 nm (Figure 3b, left). For each sample, we observe an asymmetric peak, which has the characteristic Fano lineshape.[26] The extracted Q factor is $Q = 35 \pm 5$ (see Supporting Information). We note that although this Q factor is not exceptionally high, it is sufficient to fully utilize the bandwidth of our fs pulsed pump and to implement a reasonable range of values for the asymmetry parameter α, thus ensuring optimal SHG enhancement in the pulsed regime.

To find the optimal sample, we perform SH spectroscopy of fabricated Si metasurfaces (Figure 3b, right). The observed SH signal is enabled by the artificial asymmetry of the

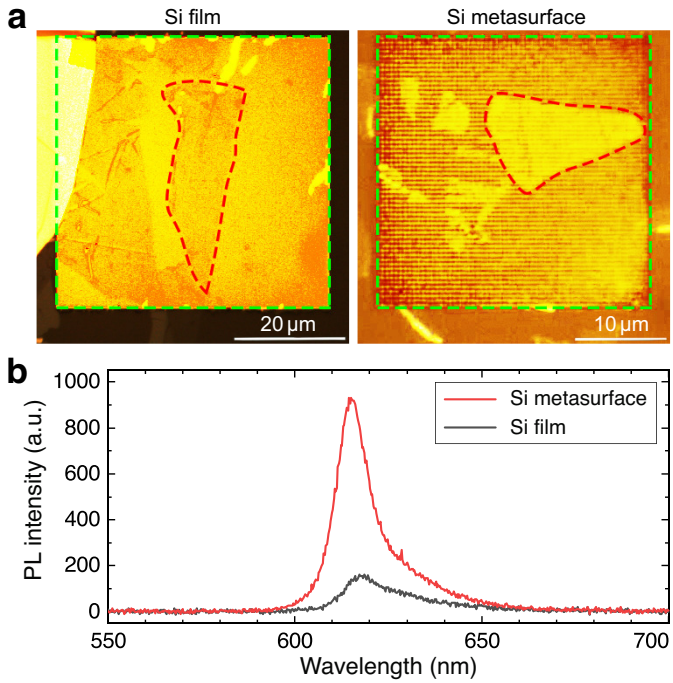

Figure 4: (a) Optical microscope images (reflected white light) of the bulk Si film (left) and metasurface (right) squares after the transfer of monolayer WS_2 flakes. The outlines of the Si structure are shown with green dashed lines and those of the flakes with red dashed lines. (b) PL spectra of the WS_2 flakes described in (a).

unit cell. The SH intensity is proportional to $|u|^4$ and reaches the maximum in the critical coupling regime. The sample with 140 nm bar width ($\alpha = 0.22$) exhibits the highest SH intensity with the peak value precisely at the wavelength of the quasi-BIC, which, within the fabrication accuracy of about ± 10 nm, agrees well with the simulations. We note, if the critical coupling regime is realized for this sample, then the peak value of SH intensity must decrease for samples with the bar width larger than 140 nm. To test this, we fabricated a set of samples with smaller asymmetry parameters and measured the corresponding SH spectra (see Supporting Information). The SH spectroscopy of the extended set of metasurfaces confirms that the critical coupling is realized for the sample with a bar width of about 140 nm.

Next, we transfer mechanically exfoliated monolayer WS_2 flakes onto the optimized metasurface sample and the reference Si film. Figure 4a shows optical microscope images of samples after the flake transfer. Both the reference Si film and metasurface are partially covered

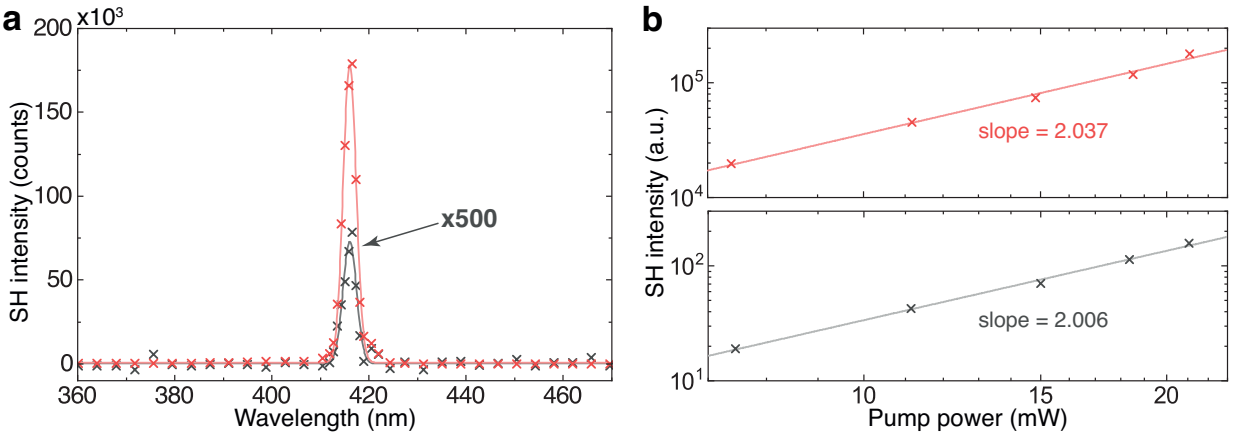

Figure 5: (a) The measured SH intensity spectrum from WS_2 monolayers on top of the optimized metasurface and on top of the reference Si film with a pump wavelength of 832 nm. Metasurface (red) and bulk Si film (gray, magnified ×500). (b) Measured SH intensity versus the pump power for WS_2 monolayers on top of the metasurface (red) and bulk Si film (gray) ($\log_{10}$ – $\log_{10}$ scale).

by large uniform flakes of about 40 µm × 16 µm and 17 µm × 11 µm size, respectively. Our transfer method ensures that these flakes are clean and have identical thickness, as we substantiate below. The quality and the number of layers in the flakes are verified with the corresponding PL spectra (Figure 4b). For both structures, the PL spectra demonstrate a direct exciton peak at the wavelength of 615 nm, while for the metasurface, the maximal intensity is about 5 times higher. The metasurface has not been designed to feature a strong resonance at this wavelength; hence, the amplification is modest. The PL signal provides us an unequivocal proof of monolayer structure of the WS_2 flake,[35] while identifying the number of layers of TMD samples through the use of atomic force microscopy[36] and Raman spectroscopy[37] requires an analysis of the complicated interplay between multiple parameters. In particular, the shape of the observed PL spectra is an essential signature of the WS_2 monolayer because, for more than one WS_2 layer, the PL spectrum shows at least one order of magnitude decrease in intensity and also exhibits an indirect excitonic emission peak at about 700 nm.[38]

To characterize the SH response of the WS_2 flake placed on top of Si structures, we illuminate the flakes at the fixed wavelength of 832 nm with laser pulses of 80 fs duration and

22 mW average pump power. We increase the efficiency of coupling between the pump and the quasi-BIC resonance by increasing the spot diameter to about 12 µm, which is comparable to the size of the flakes. Figure 5a shows a comparison between reflected SH spectra of WS_2 monolayers on top of the metasurface and on top of the reference film. We observe the SHG enhancement of about 1140 times for the 2D material on the resonant Si metasurface compared to a bulk Si film. This enhancement metric may be particularly useful in silicon photonics and meta-optics, since both rely on nano-structuring thin silicone films on low-index substrates. We note that the intrinsic SH signal of the bare metasurface is 360 times lower than that of a hybrid metasurface, and it can, therefore, be neglected (Figure 3b).

In the critical coupling regime, the SHG enhancement is proportional to the square of the Q factor (see Supporting Information), which is in perfect agreement with the measured $Q \simeq 35$. We note that the measured value of the Q factor is optimized for the current excitation setup because it is comparable to the effective Q factor of the laser pulse equal to 90 (see Supporting Information). Furthermore, Eq. (2) shows the highest SHG can be achieved via optimization of the relative rates of losses rather than maximization of the total Q factor. For $\alpha = 0$, the Q factor is maximal, while the field enhancement is zero, and for the critical coupling regime, the Q factor is not maximal, but the field enhancement is the highest. The resonant properties of the metasurface at the SH wavelength also shape the SH intensity.[25] However, for wavelengths below 500 nm, SH resonances are smeared out by strong absorption losses of Si and WS_2.[34] Finally, we conduct an experimental verification of the SH origin of the observed signal by detecting the average pump power incident on the sample and average SH power captured by the collection objective. Figure 5b shows that power-to-power dependence demonstrates an explicit quadratic behavior for both samples, which points to the SHG regime before saturation.

Conclusion

Our results demonstrate, for the first time to our knowledge, a strong enhancement of nonlinear response from a hybrid structure of a 2D monolayer combined with a resonant dielectric metasurface. The magnitude of SHG from a WS_2 monolayer on an engineered asymmetric silicon metasurface has been directly shown to be at least 1140 times higher compared to that from a WS_2 monolayer on a silicon film of the same thickness. The observed enhancement has been boosted by optical bound states in the continuum, and it is more than one and a half orders of magnitude higher than earlier reported for resonant dielectric metasurfaces. Hybrid metasurfaces supporting quasi-BIC resonances integrated with TMD monolayers promise a range of novel applications for optoelectronics and nonlinear microscopy.

Acknowledgement

Financial support was provided by the Australian Research Council (DE180100070 and DP150102071), the University of Technology Sydney (Seed Funding Grant), the Strategic Fund of the Australian National University, and the Russian Foundation for Basic Research (19-02-00419 and 19-32-90106). K.K. acknowledges support from the Foundation for the Advancement of Theoretical Physics and Mathematics "BASIS".

Supporting Information Available

The Supporting Information is available free of charge at [?]. Materials and methods, additional details on numerical methods, sample fabrication, optical setup, 2D material transfer, photoluminescence characterization, linear and nonlinear optical measurements, temporal coupled-mode theory analysis, laser bandwidth optimization, second-harmonic spectroscopy of an extended set of samples.

References

(1) Bhimanapati, G. R.; Lin, Z.; Meunier, V.; Jung, Y.; Cha, J.; Das, S.; Xiao, D.; Son, Y.; Strano, M. S.; Cooper, V. R., et al. Recent advances in two-dimensional materials beyond graphene. *ACS Nano* **2015**, *9*, 11509–11539.

(2) Mak, K. F.; Shan, J. Photonics and optoelectronics of 2D semiconductor transition metal dichalcogenides. *Nature Photonics* **2016**, *10*, 216.

(3) Wang, G.; Chernikov, A.; Glazov, M. M.; Heinz, T. F.; Marie, X.; Amand, T.; Urbaszek, B. Colloquium: Excitons in atomically thin transition metal dichalcogenides. *Reviews of Modern Physics* **2018**, *90*, 021001.

(4) Schaibley, J. R.; Yu, H.; Clark, G.; Rivera, P.; Ross, J. S.; Seyler, K. L.; Yao, W.; Xu, X. Valleytronics in 2D materials. *Nature Reviews Materials* **2016**, *1*, 1–15.

(5) Yin, X.; Ye, Z.; Chenet, D. A.; Ye, Y.; O'Brien, K.; Hone, J. C.; Zhang, X. Edge nonlinear optics on a MoS_2 atomic monolayer. *Science* **2014**, *344*, 488–490.

(6) Janisch, C.; Wang, Y.; Ma, D.; Mehta, N.; Elías, A. L.; Perea-López, N.; Terrones, M.; Crespi, V.; Liu, Z. Extraordinary second-harmonic generation in tungsten disulfide monolayers. *Scientific Reports* **2014**, *4*, 5530.

(7) Wen, X.; Gong, Z.; Li, D. Nonlinear optics of two-dimensional transition metal dichalcogenides. *InfoMat* **2019**, *1*, 317–337.

(8) Dasgupta, A.; Gao, J.; Yang, X. Atomically Thin Nonlinear Transition Metal Dichalcogenide Holograms. *Nano Letters* **2019**, *19*, 6511–6516, PMID: 31419147.

(9) Li, Y.; Rao, Y.; Mak, K. F.; You, Y.; Wang, S.; Dean, C. R.; Heinz, T. F. Probing symmetry properties of few-layer MoS_2 and h-BN by optical second-harmonic generation. *Nano Letters* **2013**, *13*, 3329–3333.

(10) Kim, S.; Fröch, J. E.; Gardner, A.; Li, C.; Aharonovich, I.; Solntsev, A. S. Second-harmonic generation in multilayer hexagonal boron nitride flakes. *Optics Letters* **2019**, *44*, 5792–5795.

(11) Carvalho, B. R.; Wang, Y.; Fujisawa, K.; Zhang, T.; Kahn, E.; Bilgin, I.; Ajayan, P. M.; de Paula, A. M.; Pimenta, M. A.; Kar, S.; Crespi, V. H.; Terrones, M.; Malard, L. M. Nonlinear Dark-Field Imaging of One-Dimensional Defects in Monolayer Dichalcogenides. *Nano Letters* **2020**, *20*, 284–291, PMID: 31794217.

(12) Cunha, R.; Cadore, A.; Ramos, S. L. L. M.; Watanabe, K.; Taniguchi, T.; Kim, S.; Solntsev, A. S.; Aharonovich, I.; Malard, L. M. Second-harmonic generation in defective hexagonal boron nitride. *Journal of Physics: Condensed Matter* **2020**, *32*, 19LT01.

(13) Fryett, T.; Zhan, A.; Majumdar, A. Cavity nonlinear optics with layered materials. *Nanophotonics* **2017**, *7*, 355, 2.

(14) Chen, H.; Corboliou, V.; Solntsev, A. S.; Choi, D.-Y.; Vincenti, M. A.; de Ceglia, D.; de Angelis, C.; Lu, Y.; Neshev, D. N. Enhanced second-harmonic generation from two-dimensional $MoSe_2$ on a silicon waveguide. *Light: Science & Applications* **2017**, *6*, e17060–e17060.

(15) Autere, A.; Jussila, H.; Dai, Y.; Wang, Y.; Lipsanen, H.; Sun, Z. Nonlinear optics with 2D layered materials. *Advanced Materials* **2018**, *30*, 1705963.

(16) Han, X.; Wang, K.; Persaud, P. D.; Xing, X.; Liu, W.; Long, H.; Li, F.; Wang, B.; Singh, M. R.; Lu, P. Harmonic Resonance Enhanced Second-Harmonic Generation in the Monolayer WS_2–Ag Nanocavity. *ACS Photonics* **2020**, *7*, 562–568.

(17) Lin, D.; Fan, P.; Hasman, E.; Brongersma, M. L. Dielectric gradient metasurface optical elements. *Science* **2014**, *345*, 298–302.

(18) Kruk, S.; Kivshar, Y. Functional meta-optics and nanophotonics governed by Mie resonances. *ACS Photonics* **2017**, *4*, 2638–2649.

(19) Tiguntseva, E.; Koshelev, K.; Furasova, A.; Tonkaev, P.; Mikhailovskii, V.; Ushakova, E. V.; Baranov, D. G.; Shegai, T.; Zakhidov, A. A.; Kivshar, Y.; Makarov, S. V. Room-Temperature Lasing from Mie-Resonant Nonplasmonic Nanoparticles. *ACS Nano* **2020**, DOI: 10.1021/acsnano.0c01468.

(20) Hsu, C. W.; Zhen, B.; Stone, A. D.; Joannopoulos, J. D.; Soljačić, M. Bound states in the continuum. *Nature Reviews Materials* **2016**, *1*, 1–13.

(21) Koshelev, K.; Bogdanov, A.; Kivshar, Y. Engineering with bound states in the continuum. *Optics and Photonics News* **2020**, *31*, 38–45.

(22) Hsu, C. W.; Zhen, B.; Lee, J.; Chua, S.-L.; Johnson, S. G.; Joannopoulos, J. D.; Soljačić, M. Observation of trapped light within the radiation continuum. *Nature* **2013**, *499*, 188–191.

(23) Rybin, M. V.; Koshelev, K. L.; Sadrieva, Z. F.; Samusev, K. B.; Bogdanov, A. A.; Limonov, M. F.; Kivshar, Y. S. High-Q supercavity modes in subwavelength dielectric resonators. *Physical Review Letters* **2017**, *119*, 243901.

(24) Jin, J.; Yin, X.; Ni, L.; Soljačić, M.; Zhen, B.; Peng, C. Topologically enabled ultrahigh-Q guided resonances robust to out-of-plane scattering. *Nature* **2019**, *574*, 501–504.

(25) Koshelev, K.; Kruk, S.; Melik-Gaykazyan, E.; Choi, J.-H.; Bogdanov, A.; Park, H.-G.; Kivshar, Y. Subwavelength dielectric resonators for nonlinear nanophotonics. *Science* **2020**, *367*, 288–292.

(26) Koshelev, K.; Lepeshov, S.; Liu, M.; Bogdanov, A.; Kivshar, Y. Asymmetric metasurfaces with high–Q resonances governed by bound states in the continuum. *Physical Review Letters* **2018**, *121*, 193903.

(27) Koshelev, K.; Tang, Y.; Li, K.; Choi, D.-Y.; Li, G.; Kivshar, Y. Nonlinear Metasurfaces Governed by Bound States in the Continuum. *ACS Photonics* **2019**, *6*, 1639–1644.

(28) Yuan, Q.; Fang, L.; Fang, H.; Li, J.; Wang, T.; Jie, W.; Zhao, J.; Gan, X. Second-harmonic and sum-frequency generations from a silicon metasurface integrated with a two-dimensional material. *ACS Photonics* **2019**, *6*, 2252–2259.

(29) You, J. W.; Bongu, S. R.; Bao, Q.; Panoiu, N. C. Nonlinear optical properties and applications of 2D materials: theoretical and experimental aspects. *Nanophotonics* **2018**, *8*, 63, 1.

(30) Jia, B. 2D optical materials and the implications for photonics. *APL Photonics* **2019**, *4*, 080401.

(31) Maier, S. A. Plasmonic field enhancement and SERS in the effective mode volume picture. *Optics Express* **2006**, *14*, 1957–1964.

(32) Sadrieva, Z. F.; Sinev, I. S.; Koshelev, K. L.; Samusev, A.; Iorsh, I. V.; Takayama, O.; Malureanu, R.; Bogdanov, A. A.; Lavrinenko, A. V. Transition from optical bound states in the continuum to leaky resonances: Role of substrate and roughness. *ACS Photonics* **2017**, *4*, 723–727.

(33) Fan, S.; Suh, W.; Joannopoulos, J. D. Temporal coupled-mode theory for the Fano resonance in optical resonators. *JOSA A* **2003**, *20*, 569–572.

(34) Zhao, W.; Ghorannevis, Z.; Chu, L.; Toh, M.; Kloc, C.; Tan, P.-H.; Eda, G. Evolution of electronic structure in atomically thin sheets of WS2 and WSe2. *ACS nano* **2013**, *7*, 791–797.

(35) Gutiérrez, H. R.; Perea-López, N.; Elías, A. L.; Berkdemir, A.; Wang, B.; Lv, R.; López-Urías, F.; Crespi, V. H.; Terrones, H.; Terrones, M. Extraordinary room-temperature photoluminescence in triangular WS2 monolayers. *Nano letters* **2013**, *13*, 3447–3454.

(36) Tan, C.; Cao, X.; Wu, X.-J.; He, Q.; Yang, J.; Zhang, X.; Chen, J.; Zhao, W.; Han, S.; Nam, G.-H., et al. Recent advances in ultrathin two-dimensional nanomaterials. *Chemical reviews* **2017**, *117*, 6225–6331.

(37) Berkdemir, A.; Gutiérrez, H. R.; Botello-Méndez, A. R.; Perea-López, N.; Elías, A. L.; Chia, C.-I.; Wang, B.; Crespi, V. H.; López-Urías, F.; Charlier, J.-C., et al. Identification of individual and few layers of WS_2 using Raman spectroscopy. *Scientific reports* **2013**, *3*, 1755.

(38) Zeng, H.; Liu, G.-B.; Dai, J.; Yan, Y.; Zhu, B.; He, R.; Xie, L.; Xu, S.; Chen, X.; Yao, W.; Cui, X. Optical signature of symmetry variations and spin-valley coupling in atomically thin tungsten dichalcogenides. *Scientific Reports* **2013**, *3*, 1608.